Optics and Lasers in Engineering 189 (2025) 108914

Contents lists available at ScienceDirect

Optics and Lasers in Engineering

journal homepage: www.elsevier.com/locate/optlaseng

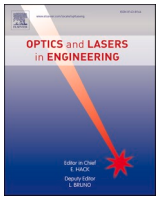

Precision displacement measurement via sampling moiré method with advanced image stabilization

Shien Ri [a,b,*], Hiroto Oouchi [a,b], Jiaxing Ye [a], M.J. Mohammad Fikry [b], Shinji Ogihara [b]

[a] Research Institute for Measurement and Analytical Instrumentation, National Institute of Advanced Industrial Science and Technology, Tsukuba, Ibaraki 305-8568, Japan
[b] Department of Mechanical and Aerospace Engineering, Tokyo University of Science, Noda City, Chiba 278-8510, Japan

ARTICLE INFO

Keywords:
Displacement measurement
Sampling moiré
Phase information
Image stabilization
Projective transformation

ABSTRACT

Aging infrastructure poses significant challenges for modern society and imposes substantial burdens in assessing and managing health conditions worldwide. Vision-based displacement measurement has gained considerable research interest due to its cost efficiency and high precision. This study focuses on enhancing vision-based methods in scenarios where camera motion occurs during image capture. We propose a novel approach for precise camera motion compensation, enabling accurate measurement of true structural displacements. Utilizing the sampling moiré method with sub-pixel accuracy of 1/100, we establish a robust foundation for high-precision motion compensation and displacement analysis. A novel two-stage processing framework is introduced to effectively eliminate camera-induced motion while preserving actual displacement data. To validate our method, we systematically design and conduct experiments analyzing key parameters for image stabilization, demonstrating the effectiveness of our approach through comprehensive comparisons.

1. Introduction

The displacement measurement technique, which quantifies object deformation, is increasingly applied across various fields. In structural health monitoring, it plays a crucial role in assessing the safety of infrastructure, such as bridges and tunnels, by measuring deflection and displacement. Aging infrastructure presents a major challenge worldwide, particularly for bridges. As of 2023, approximately 42 % of bridges in the United States [1] and 39 % in Japan have exceeded 50 years of age [2]. This percentage is expected to exceed 55 % by 2030 in both countries, highlighting the urgent need for effective monitoring solutions. This situation is especially critical in Japan, a seismically active nation that has experienced numerous significant earthquakes. According to the 2023 White Paper on Land, Infrastructure, Transport, and Tourism indicates that maintenance management based on preventive practices is expected to save over 6 trillion yen by fiscal year 2025, reducing costs by more than 40 % compared to reactive maintenance conducted after structural issues arise [3]. Given the impracticality of large-sale reconstruction, there is an increasing demand for efficient, non-destructive evaluation methods to ensue structural safety and longevity.

Bridges, the focal point of this investigation, endure various loads from traffic, strong wind (typhoon), and temperature fluctuations, leading to vertical displacements (i.e., deflection). Measurement of these displacements offers a non-destructive means to assess bridge safety. Various methods have been investigated for sensor-based deflection measurement, including accelerometers [4], strain gauges [5], inclinometers [6], total stations [7], fiber Bragg grating sensors [8], laser Doppler systems [9], and laser scanning [10]. Despite their potential, these methods face significant implementation challenges, such as high installation costs and limited usability in specific measurement environments. In recent years, there has been significant interest in using digital imaging to measure displacement and strain in both large-scale [11–14] and small-scale structures [15–18]. This optical method relies on tracking target points such as speckles [19] or regular grating patterns [20] within images. Numerous techniques have been developed for this purpose [21–25]. These methods utilize digital imagery, advanced computer vision techniques, and regular pattern phase analysis for precise tracking and phase measurement [26–28]. Recently, a deep learning approach for measuring structure displacements has been proposed [29,30].

The optical displacement measurement methods discussed thus far rely on the assumption that images are acquired using a camera

* Corresponding author at: Research Institute for Measurement and Analytical Instrumentation, National Institute of Advanced Industrial Science and Technology, Tsukuba, Ibaraki 305-8568, Japan.
E-mail address: ri-shien@aist.go.jp (S. Ri).

https://doi.org/10.1016/j.optlaseng.2025.108914
Received 29 December 2024; Received in revised form 19 February 2025; Accepted 23 February 2025
Available online 8 March 2025

mounted on a stationary platform, such as a tripod. However, practical implementations may encounter significant challenges when no stable mounting spot is available. Researchers have proposed various camera motion compensation techniques to overcome these limitations and enable more flexible and low-cost structural displacement measurement by using handheld camera [31] and drones [32–36]. Jana et al. [37] (2021) employed an affine transformation matrix to estimate the camera rotation matrix induced by motion. Similarly, planar homography, which is also known as perspective transformation, was adopted for camera motion compensation by Lavezzi et al. [38]. On the other hand, since the compensation performance is determined by the precision of input coordinates of motion trackers, more recent studies have gathered the utilization of phase-based methods to attain more accurate coordinates measurements [39,40]. In addition to vision-based solutions, Y. Zhang et al. [41] and Weng et al. [31] have developed multimodal compensation approaches for the camera movement by using an attached tilt sensor and an inertial measuring unit (IMU), respectively. This approach, however, requires additional sensor inputs, which can be a burden for additional data processing and fusion.

This research addresses the critical challenge of mitigating camera movement effects to achieve robust displacement measurement, enabling the use of flexible, low-cost devices such as handheld camera, smartphones and drones (Fig. 1). To accomplish this, we integrate a displacement measurement approach based on the sampling moiré method [42–45] with a novel image stabilization technique developed in this study. We hypothesize that the high-precision trajectory estimations of trackers analyzed by sampling moiré significantly enhance compensation performance. Our unique image stabilization method mitigates camera-induced motion by applying a secondary projection transformation with 1/100 pixels precision, complementing the initial pixel-level projection transformation. This integrated system enables highly accurate displacement measurements. Theoretical analyses, along with systematic experimental validations, including parameter analyses and comparative evaluations, confirm the efficacy of the proposed method.

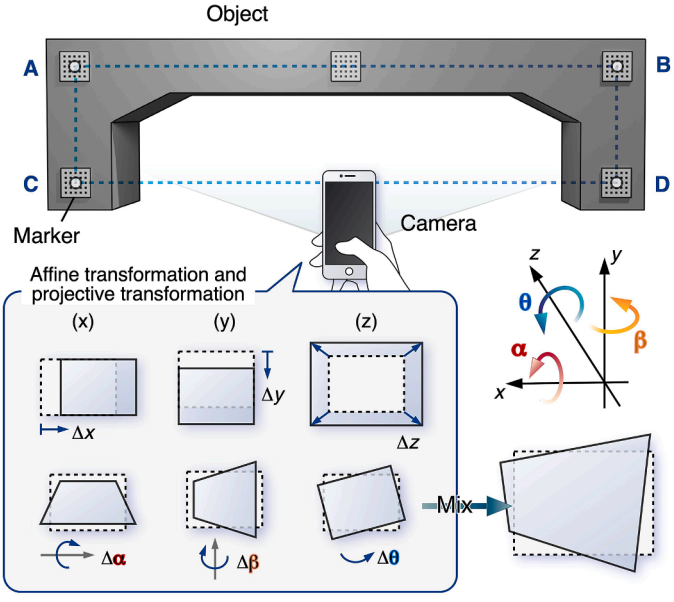

Fig. 1. Overview of this research on image displacement measurement using handheld photography without the camera being fixed on a tripod.

2. Principle of displacement measurement

2.1. Outline of sampling moiré method

The sampling moiré method [42–44] is a technique that generates a series of moiré images by processing a single captured grating image through down-sampling and intensity interpolation. This approach enables the extraction of the phase distribution of the original grating image from the generated moiré images, as illustrated in Fig. 2.

The process begins with acquiring an image of the periodic pattern. In the SM method, the intensity distribution of a 1D or 2D grating $f(x, y)$, characterized by a pitch p (in millimeters) and an initial phase φ_0, can be mathematically expressed by Eq. (1) when recorded with a camera.

$$\begin{aligned} f(x,y) &= a(x,y)\cos\left\{2\pi\frac{x}{P}+\varphi_0\right\}+b(x,y) \\ &= a(x,y)\cos\{\varphi(x,y)\}+b(x,y) \end{aligned} \tag{1}$$

where $a(x, y)$ represents the amplitude of the grating intensity, while $b(x, y)$ corresponds to the background intensity. The parameter P denotes the grating pitch recorded in pixel units on the image plane, and φ represents the phase value of the grating. Since the same grating pitch in the x- and y-directions is used in typical experiments, P_x and P_y are expressed as P for simplicity.

Then, by applying down-sampling with an integer sampling pitch of T-pixel and incorporating intensity interpolation, multiple phase-shifted fringe patterns, denoted as $f_m(x, y; k)$, can be obtained and these phase-shifted patterns are mathematically expressed as follows:

$$\begin{aligned} f_m(x,y;k) &= a(x,y)\cos\left\{2\pi\left(\frac{1}{P}-\frac{1}{T}\right)x+\varphi_0+2\pi\frac{k}{T}\right\}+b(x,y) \\ &= a(x,y)\cos\left\{\varphi_m(x,y)+2\pi\frac{k}{T}\right\}+b(x,y),(k=0,1,\cdots,T-1) \end{aligned} \tag{2}$$

The phase distribution of the moiré fringe, $\varphi_m(x, y)$, can be derived using the phase-shifting method with the Discrete Fourier Transform (DFT) algorithm, as represented by Eq. (3).

$$\varphi_m(x,y) = -\tan^{-1}\frac{\sum_{k=0}^{T-1} f_m(x,y;k)\sin(2\pi k/T)}{\sum_{k=0}^{T-1} f_m(x,y;k)\cos(2\pi k/T)} \tag{3}$$

Similarly, moiré fringe's phase distribution after deformation can be evaluated using the same Eq. (3). Subsequently, the in-plane displacement is directly derived from the phase difference distribution of the moiré fringe before and after deformation.

$$\delta(x,y) = -\frac{p}{2\pi}\Delta\varphi_m(x,y) \tag{4}$$

In the SM method, the step of phase analysis using the DFT algorithm ensures a high level of precision. As a result, the in-plane displacement is calculated based on the phase difference of the moiré fringe captured before and after deformation, achieving an accuracy of 1/100 pixel or 1/1000th of the grating pitch. Besides, it is important to highlight that the SM method provides both precise displacement calculations and image stabilization in our proposed technique.

While the sampling moiré method offers a fast and precise means of measuring displacements, its accuracy is significantly impacted by camera motion. The key challenges include:

1) *Displacement and Direction Ambiguity*: Since phase extraction relies on a periodic pattern, determining the absolute displacement and direction beyond half the grating pitch is difficult. As a result, accurately measuring small displacements becomes challenging due to camera movement.
2) *Breakage of Periodicity*: Out-of-plane rotation of the captured marker image disrupts the periodicity of the pattern, leading to errors in phase calculation.

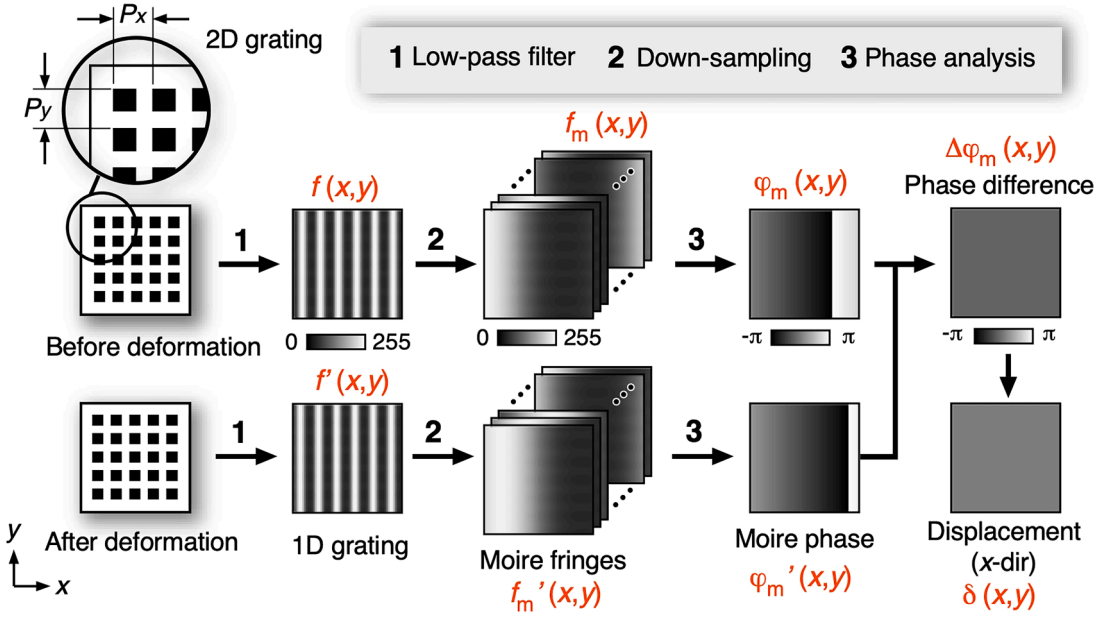

Fig. 2. Principle of the sampling moiré method for small displacement measurement using a regular grating pattern.

To overcome these challenges, this study introduces an image correction approach based on image stabilization using four reference markers. This method ensures precise displacement measurements with the sampling moiré technique, even in the presence of camera motion.

2.2. Advanced image stabilization

In this study, we present a novel image correction technique employing projective transformation to mitigate the effects of three-dimensional camera motion. Projective transformation is a geometric operation that rectifies tilted planes, converting them into a frontal perspective for accurate analysis. The fundamental equation governing this transformation is given by Eq. (5), where x and y represent the original coordinates, and x' and y' denote the coordinates transformed coordinates. The coefficients a, b, and c are the unknown parameters of the transformation matrix, which are determined to achieve precise image correction.

$$x' = \frac{a_1 x + b_1 y + c_1}{a_0 x + b_0 y + 1}$$
$$y' = \frac{a_2 x + b_2 y + c_2}{a_0 x + b_0 y + 1} \tag{5}$$

In practical applications, the actual coordinates of reference points are recorded both before and after the transformation, enabling the determination of the transformation coefficients. Since projective transformation involves eight undetermined coefficients, it requires the coordinates of at least four points before and after transformation. In this study, we utilize the *cv2.getPerspectiveTransform()* function in OpenCV for perspective transformation applying linear intensity interpolation. Given that the sampling moiré method relies on low-frequency moiré fringes generated through down-sampling, interpolation-induced errors are negligible. However, directly applying projective transformation within the sampling moiré method does not achieve optimal precision. To enhance accuracy, we propose a two-stage image correction approach. In the first stage, initial coarse positioning is performed using standard projective transformation. In the second stage, we refine the positioning to sub-pixel accuracy by precisely determining reference point coordinates through the sampling moiré method, achieving a precision of 1/100 of a pixel. This dual-phase strategy effectively corrects images while preserving the high-precision displacement measurement capabilities of the sampling moiré method.

Fig. 3 illustrates the principle of advanced image stabilization using a two-stage projective transformation with sub-pixel accuracy. Fig. 3(a) shows the capturing recorded images of four reference points before deformation and after deformation, highlighting image blurring caused by camera rotation; Fig. 3(b) presents the two-stage projective transformation consisting of an initial perspective projection achieved with pixel-level accuracy using automatic detection of the center coordinates

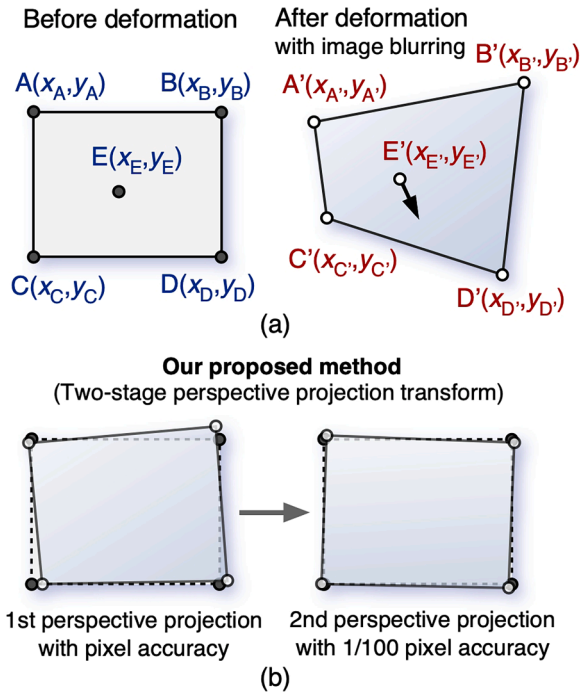

Fig. 3. Principle of the advanced image stabilization: (a) capturing recorded images of four reference points both before deformation and after deformation, taking into account the image blurring caused by camera rotation, and (b) two-stage projective transformation consisting of an initial perspective projection with pixel-level accuracy, followed by a second perspective projection with an accuracy of 1/100-pixel.

of circular markers, followed by a second perspective projection with 1/100-pixel accuracy utilizing grating markers and the sampling moiré method.

The initial projective transformation provides coarse alignment at the pixel level, enabling image correction within half a pitch of the regularity pattern. This correction enables accurate detection of small displacements using the sampling moiré method. Following this, the displacements of the moiré markers placed around the reference points are measured. Although the initial projective transformation aligns the reference points, the measured displacements of the moiré markers typically do not register as zero due to residual errors. To further enhance accuracy, each measured displacement is combined with the reference point coordinates, enabling sub-pixel precision. These refined coordinates are then applied in a secondary projective transformation, achieving image correction at 1/100-pixel precision. This innovative two-stage projective transform method represents a novel advancement in high-precision image stabilization, offering a level of accuracy not yet addressed in existing literature.

As explained earlier, the use of four reference points is essential for performing the projective transformation. In this study, the center of each circle is automatically detected and used as the reference point. Since the markers used in the sampling moiré method are square, it is necessary to introduce dimensionless parameters to distinguish them from circles. Herein, the following dimensionless parameter W is introduced:

$$W = \frac{4\pi S}{L^2} \tag{6}$$

where S represents the area enclosed by a contour and L signifies the perimeter surrounding it. For an ideal circle, W equal to 1, while for a square, W is approximately 0.78. By setting a threshold between these two values, we can effectively detect only circles and ellipses. In this study, we used a threshold of $W = 0.84$ to identify circles.

Fig. 4 illustrates the process of detecting circles and ellipses in a simulated grating image. In Fig. 4**(a)**, the original image shows a marker that has been rotated by 20 ° both horizontally and vertically. Fig. 4**(b)** displays the detected contours, while Fig. 4**(c)** presents the centers of the four detected circles.

The flowchart in Fig. 5 illustrates the step-by-step process of our proposed image correction methodology. The process begins with the acquisition of image or video footage, which provides the time-series image data as input. The final displacement is then calculated and exported while compensating for image blurring. The workflow of our method includes the following three main steps:

- **Step 1: Initial image stabilization**
  Detect the center coordinates of four reference markers with pixel-level precision. Apply a projective transform to achieve pixel-level accuracy, reducing image blurring at a coarse level.
- **Step 2: Sub-pixel Refinement**
  Use the sampling moiré method to calculate the displacements of the moiré markers with sub-pixel precision. Perform a fine image stabilization using a second projective transform, based on the refined marker center coordinates from the sampling moiré method.
- **Step 3: Final Displacement Calculation**
  After the two-stage image stabilization process, compute the final displacement with improved accuracy, ensuring that image blurring effects are minimized.

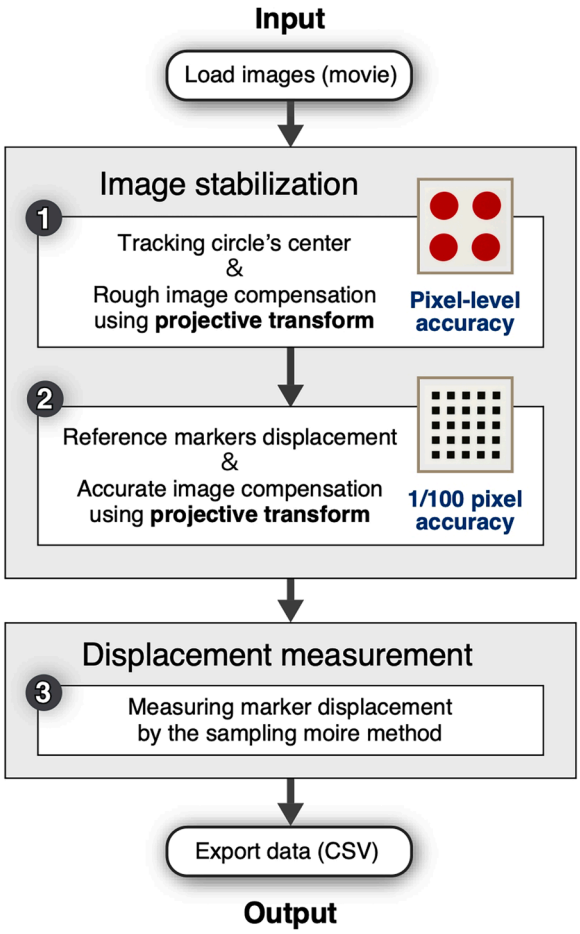

Fig. 5. Flowchart of image processing for image stabilization and accurate displacement measurement.

3. Experiment

3.1. Experimental setup

To validate the accuracy of the proposed methodology, laboratory experiments were conducted using a miniature optical setup designed to simulate bridge displacement monitoring. This setup included two

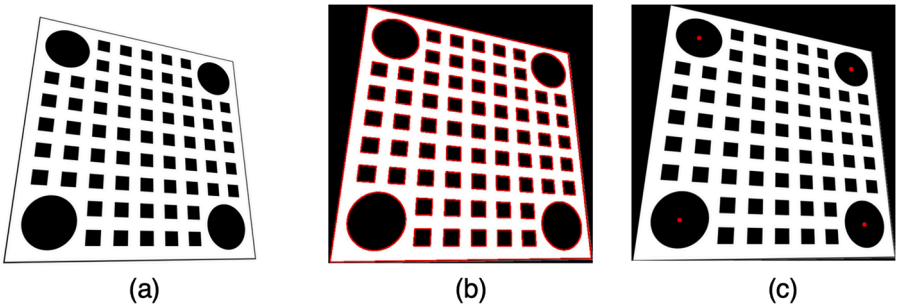

Fig. 4. Detecting the center of the circle: (a) original image, (b) detecting contours, (c) detecting results of the center of four circles.

multi-axis moving stages, enabling both displacement measurement and controlled of camera motion simulation. An overview of the optical configuration used in the experiments is shown in Fig. 6. The specifications of the equipment and the experimental conditions are detailed below. The camera-to-marker distance was set at 1.2 m.

(1) **Moiré markers:** The experiment utilizes moiré markers, consisting of a printed grid pattern with a 10 mm pitch in both the *x* and *y* directions. The desired precision of the sampling moiré method employed in this investigation is set at less than 1/500 of the grid pitch, equivalent to ±0.02 mm. Additionally, circular markers, with a 20 mm diameter were strategically placed at the four corners alongside the moiré markers. These circular markers serve as reference points for the projective transformation process in image stabilization.

(2) **Image recording:** For image acquisition, an industrial-grade Basler USB 3.0 global shutter area-scan camera (model acA4096–40 um; monochrome) was used, featuring a Sony IMX255 CMOS sensor. This camera has a 1-inch sensor with a pixel size of 3.45 μm, capturing 8-bit grayscale images at a resolution of 8.9 MP (4096 × 2168 pixels) at 42 frames per second (fps). It supports multiple synchronization modes, including free-running, hardware triggering, and software triggering, to facilitate efficient image acquisition. During the experiment, the camera was connected to and controlled by a personal computer. A 12 mm focal length lens was attached to the camera. Grating images of 4104 × 1012 pixels were recorded and saved at 10 fps, with a shutter speed of 1/80 s to record the grating image with minimal motion blur.

(3) **Dual 6-axis stage:** The experimental setup, depicted in Fig. 6, utilized a NanoMax 6-Axis Flexure Stage (Thorlabs MAX681/M) equipped with a stepping motor. A central measuring marker and a camera were mounted on the 6-axis moving stage, allowing for independent control of the target displacement (simulating bridge deflection) and camera rotation. This precision stage provides 6 degrees of freedom, with movement ranges up to 4 mm along the *X, Y*, and *Z* axes and rotational movement up to 8° for θ_x, θ_y, and θ_z. This stage featured a repetitive positioning accuracy of 1.8 nm for the X and Y axis, and 1.2 nm for the Z axis, and 0.021 μRad for rotational axes (θ_x, θ_y, and θ_z). A personal computer controlled the stage via the stage controllers, which can manage up to 12 axes. The control software allows for precise adjustments of displacement and rotation angles across both 6-axis stages.

3.2. Experimental condition

In this experiment, displacement was applied to a moving stage on which the measurement marker was placed, as shown in Fig. 7(a). The stage moved in the *y*-direction, starting from 0 mm to 1 mm over a 2 s (0–2 s) and then held at this position for another 2 s. Next, it moved from 1 mm to 2 mm over 2 s before reversing the displacement - first from 2 mm back to 1 mm and then from 1 mm to 0 mm, returning to its original position.

To simulate real-world conditions where image blurring occurs, such as drone-based and handheld photography, three different rotation cases were applied to the camera, as illustrated in Fig. 7(b). These cases involved:

(1) Small rotational movement from 0 to 0.1 °, introducing minimal motion blur.
(2) Moderate rotational movement from 0 to 1 °, simulating typical camera motion.
(3) Large rotational movement ranging from -4 to 4 °, with a maximum rotation of 8 °, to assess the impact of significant camera motion on displacement measurements.

3.3. Image compensation

In the image analysis of the sampling moiré method, a sampling pitch of 31-pixel was used, and the average value over a 100 × 100 pixel area at the center of each marker was measured. The experimental results of image stabilization are presented in Fig. 8, which examines the case when the rotation angles around the three axes (*x, y, z*) are each set to 1 °. Fig. 8**(a)** and **(b)** show the captured images before and after deformation, respectively. Fig. 8**(c)** and **(d)** display the automatic detection of the four corner reference markers' center coordinates in both the images before and after deformation. Fig. 8**(e)** depicts the image after the initial projective transformation with pixel-level accuracy, while Fig. 8**(f)** shows the image following a second projective transformation,

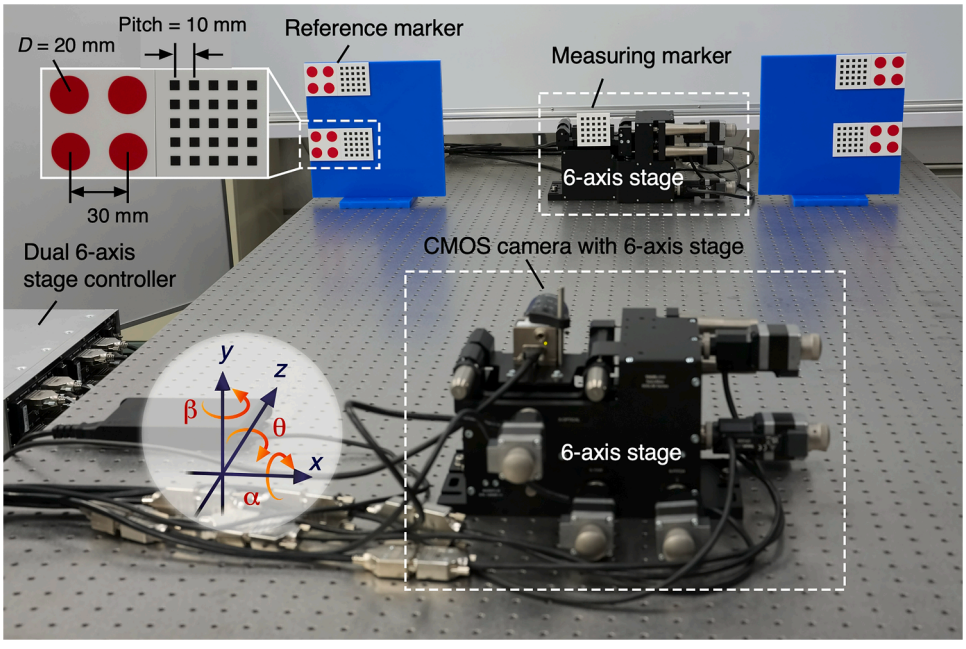

Fig. 6. Arrangement of experimental setup to verify the displacement measurement accuracy with camera rotation.

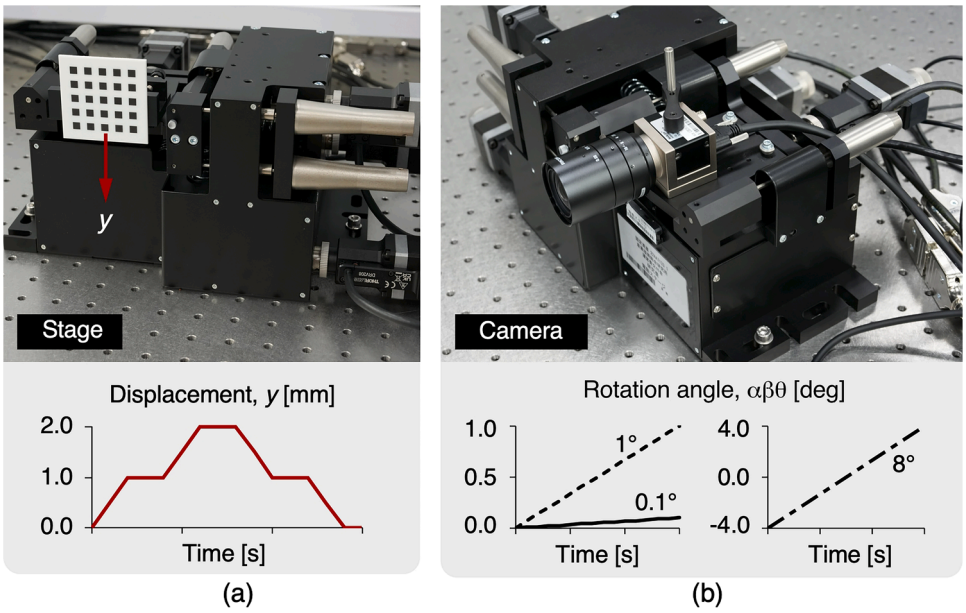

Fig. 7. Experimental condition include (a) measuring marker displacement and (b) camera rotation, which encompasses cases of 0.1 °, 1 °, and 8 ° for both single-axis and three-axis rotations.

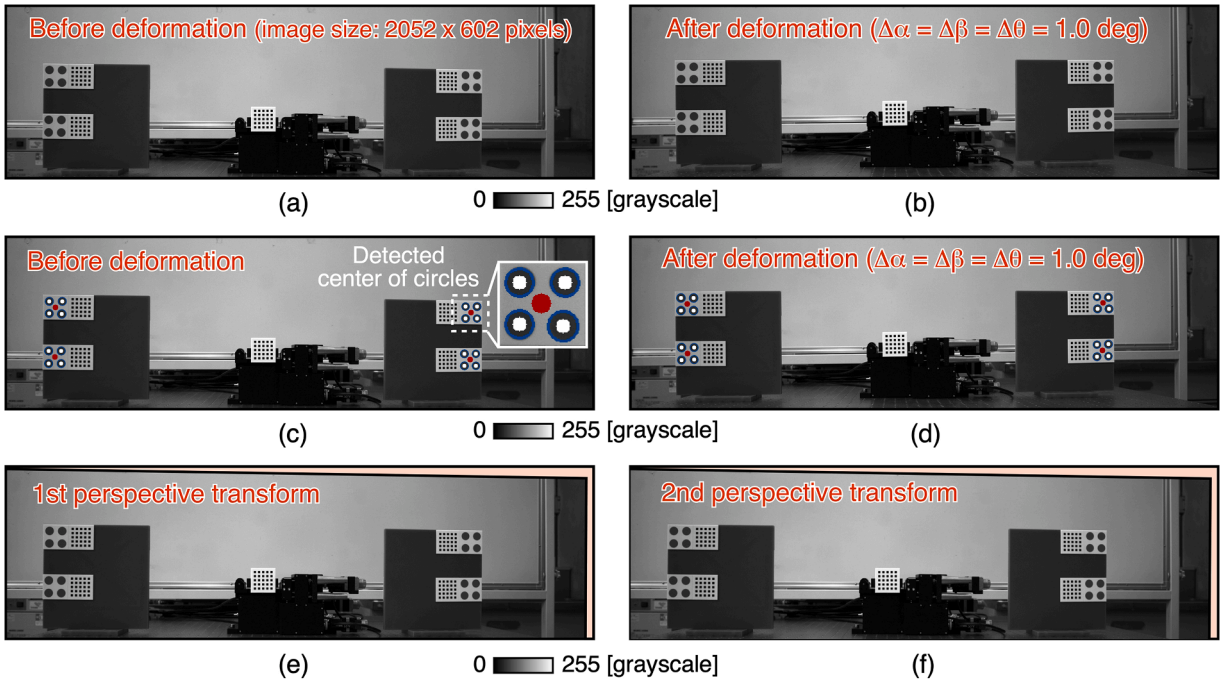

Fig. 8. Experimental results of image stabilization: (a) captured image before deformation, (b) captured image after deformation when the rotation angle αβθ of the three *xyz*-axes is 1 °, (c), (d) automatic detection results of the center coordinates of the four corner reference markers in the images before and after deformation, (e) image compensation after the first projection transformation with pixel accuracy, (f) image compensation after the second sub-pixel-precision projective transformation.

achieving sub-pixel precision.

Fig. 9 further examines the stabilization effect through a time-series analysis of the central measurement marker. It shows 200 × 200 pixel images captured every 3 s under 1 ° three-axis rotations. Since the moving stage operated at a low speed, motion blur was negligible. Fig. 9 **(a)** shows the image at 0 s as the reference for the correction. Fig. 9**(b)** displays images taken from 3 s to 15 s, while Fig. 9**(c)** shows the corrected images after applying the proposed two-stage projective transformation. The results clearly demonstrated that the blurring effect caused by three-axis camera rotation in three dimensions was significantly reduced.

Fig. 10**(a)** and **(b)** show the images captured before and after deformation under an 8 ° rotation applied simultaneously to the *x*-, *y*-, and *z*-axes. The automatic detection of the center coordinates of the four reference markers is depicted in Fig. 10**(c)** and **(d)**. Fig. 10**(e)** and **(f)** present the results of image stabilization after the initial projective transformation with pixel-level precision and the subsequent transformation with sub-pixel-precision, respectively. Despite the significant

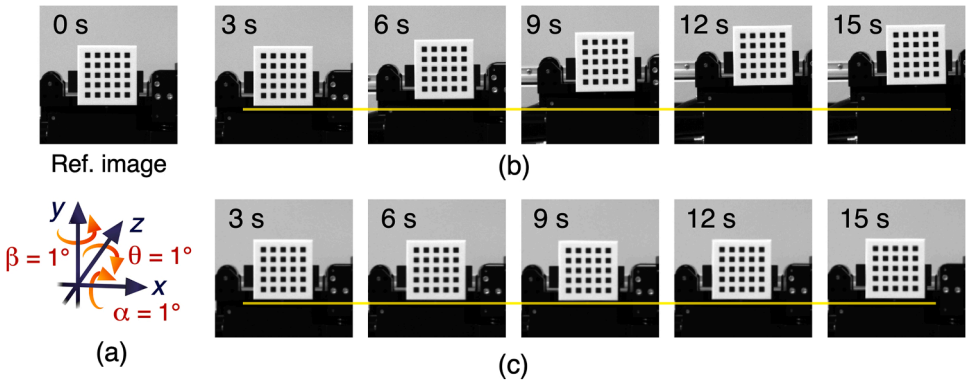

Fig. 9. Image blurring compensation in the case of 3-axis rotation was 1 °: (a) reference image at 0 s, (b) experimental images before compensation, (c) corrected images after compensation.

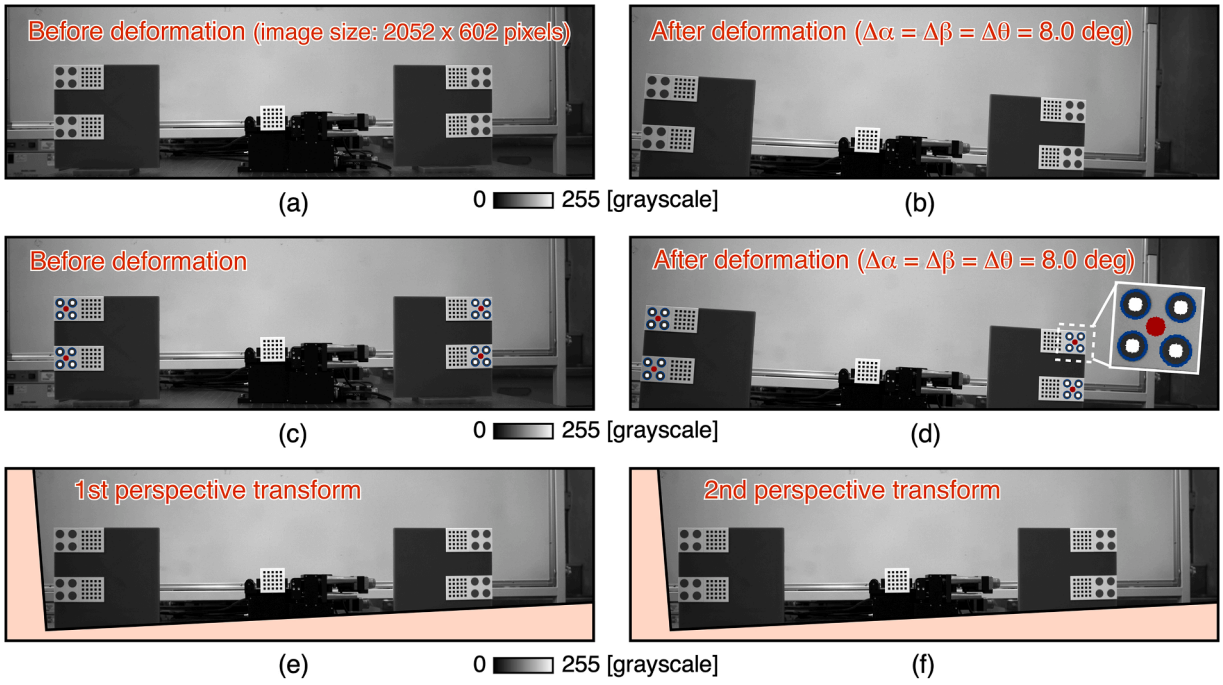

Fig. 10. Experimental results of image stabilization: (a) captured image before deformation, (b) captured image after deformation when the rotation angle αβθ of the three *xyz*-axes is 8 °, (c), (d) automatic detection results of the center coordinates of the four corner reference markers in the images before and after deformation, (e) image compensation after the first projection transformation with pixel accuracy, (f) image compensation after the second sub-pixel-precision projective transformation.

camera rotation, the effectiveness of the proposed image stabilization method is clearly demonstrated.

Fig. 11 displays images captured every 3 s (350 × 350 pixels) along with the corrected images (200 × 200 pixels) of the central measurement marker throughout the time series, with a camera rotation of 8 ° applied to all three axes. In this analysis, displacement calculation were based on the reference image taken at 9.3 s, when the marker was facing forward, rather than using the initial image at 0 s. As a result, a slight initial error was observed in the -4 ° image, as shown in Fig. 15(c).

3.4. Single-axis rotation

We first present the experimental results for micro-rotations along a single axis. Fig. 12 displays the experimental results when the camera is rotated by 0.1 ° along the *x*-axis. Figs. 12**(b)** and **(c)** compare the measured displacements obtained using the conventional sampling moiré method and the proposed image stabilization method, respectively. Without image stabilization, significant measurement errors arise due to camera rotation, preventing accurate displacement measurements. However, by applying the proposed image stabilization method, the effects of minor single-axis rotation are effectively mitigated, enabling precise displacement measurement.

Similarly, Fig. 13 shows the experimental results for a 1 ° camera rotation around the *x*-axis. As shown in Fig. 13**(b)**, when the displacement exceeds half of the grating pitch (equivalent to 5 mm in this study), the sampling moiré method becomes ineffective due to phase jumping, leading to incorrect measurement results. However, after applying the proposed image stabilization technique, the measurement results more closely aligned with the actual displacement, as shown in Fig. 13**(c)**. Despite this improvement, the impact of camera rotation was not perfectly eliminated, resulting in a residual error of 0.248 mm.

3.5. Three-axis rotation

In addition to single-axis rotation, the effect of simultaneous three-axis rotation on measurement accuracy was also investigated. Fig. 14

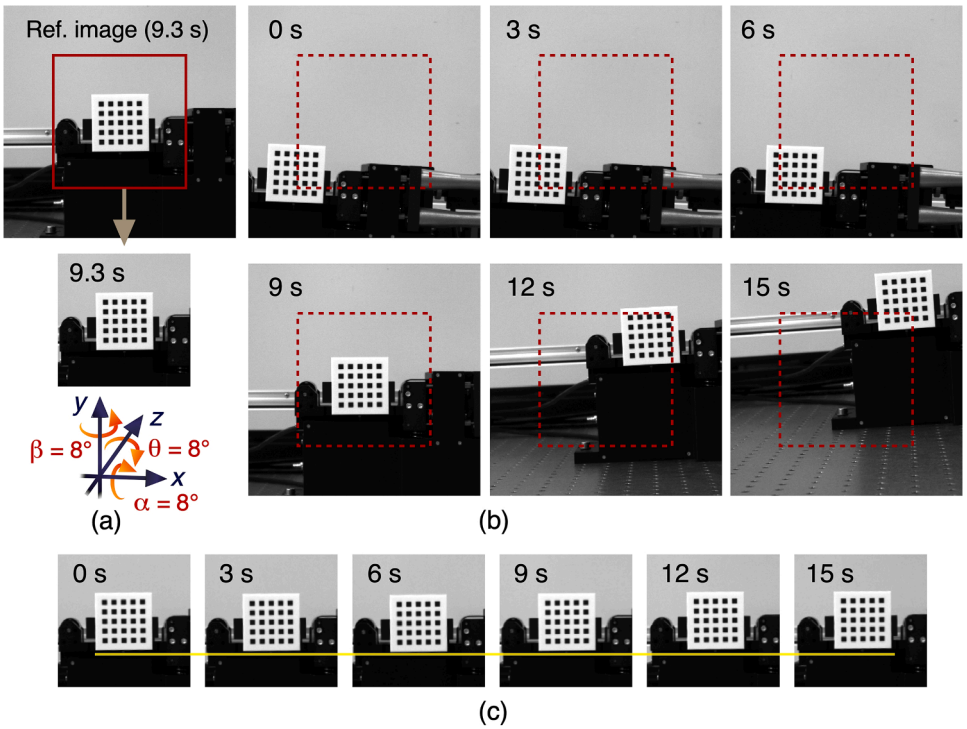

Fig. 11. Image blurring compensation in the case of 3-axis rotation was 8 °: (a) reference image at 9.3 s, (b) experimental images before compensation, (c) corrected images after compensation.

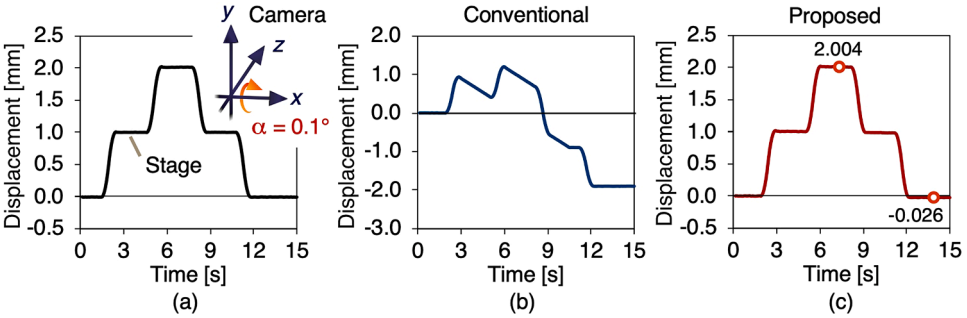

Fig. 12. Experimental results with the camera rotated for single-axis, α = 0.1 °: (a) actual displacement in *y*-direction when the camera rotation angle is 0.1 ° around *x*-axis, (b) measured displacement by conventional sampling moiré method calculation, and (c) measured displacement by the proposed method with image stabilization.

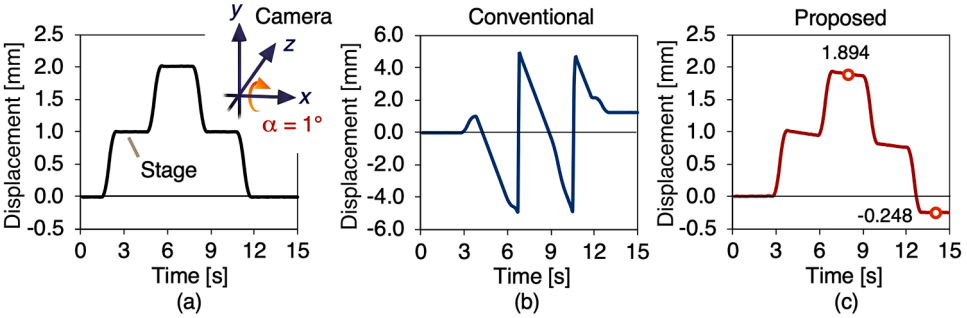

Fig. 13. Experimental results with the camera rotated for single-axis, α = 1 °: (a) actual displacement in *y*-direction when the camera rotation angle is 1 ° around *x*-axis, (b) measured displacement by conventional sampling moiré method calculation, and (c) measured displacement by the proposed method with image stabilization.

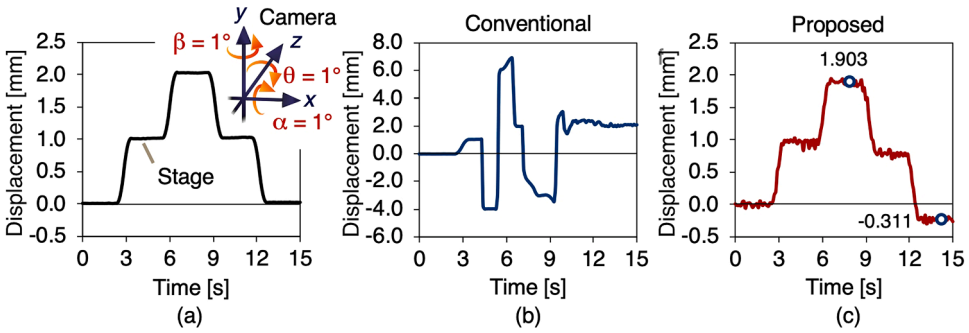

Fig. 14. Experimental results with the camera simultaneous rotated 1 ° for three-axis: (a) actual displacement in *y*-direction when the camera rotation angle is 1 ° around *xyz*-axes, (b) measured displacement by conventional sampling moiré method calculation, and (c) measured displacement by the proposed method with image stabilization.

presents the experimental results for a 1 ° camera rotation around the *x*-, *y*-, and *z*-axes simultaneously. As seen in Fig. 14**(b)**, the conventional sampling moiré method fails to provide accurate displacement measurements under these conditions. When the image stabilization method is applied, the measurement trend improves, as shown in Fig. 14**(c)**. However, the measuring error at 14 seconds was 0.311 mm, and overall variations were greater than that those observed in the single-axis case. This suggests that multi-axis rotation reduce the accuracy of the initial pixel-accuracy projective transformation, making smooth image stabilization more challenging.

Fig. 15 shows the experimental results for an 8 ° camera rotation around all three axes simultaneously. The proposed image stabilization method successfully mitigate motion effects within a range not exceeding half a period of the grating pitch, even under these challenging conditions. However, as the rotation angle increased, significant measurement errors remained after image stabilization, preventing the sampling moiré method from achieving its original accuracy. Notably, the measurement error at 14 seconds reached 1.861 mm. This suggests that the image stabilization method utilizing projective transformation proposed in this study has limitations when dealing with significant camera rotation, indicating that further improvements are necessary.

4. Discussions

Based on the accuracy verification experiments, three key perspectives are discussed.

Perspective 1. *Accuracy of the Improved Method Under Small and Large Rotational Conditions*

for a rotation of 0.1°, the proposed method achieved measurement accuracy comparable to that of the sampling moiré method, effectively compensating for micro-rotation along a single axis. However, at a larger rotation of 1.0°, there remained a residual error. This discrepancy can be attributed to the limitation of projective transformation, which approximates three-dimensional motion using a two-dimensional reference. Since a camera-captured digital image lacks depth information, the transformation process cannot fully reconstruct out-of-plane motions, leading to incomplete correction when estimating the rotation matrix.

Perspective 2. *Effects of Multi-Axis Rotations on Measurement Accuracy*

The measurement outcomes for minor rotations across the three axes were similar to those observed in the single-axis scenario, demonstrating the minimal impact of rotations outside the concerned axis within 1.0°. However, an increase in noise levels was observed across all analytical results compared to the single-axis rotation setting. When examining the post-projection transformed images, the trajectory of target markers exhibited a wiggling behavior. This behavior aligns with the previous analysis, indicating that lack of depth information from out-of-plane rotations introduces inaccuracies in projection transformation, leading to residual errors in displacement estimation.

Perspective 3. *Limitations of the Image Stabilization Method*

Ensuring the reliability of infrastructure inspection techniques is critical for maintaining structural safety. To enhance their integrity, it is essential to identify their limitation. In this study, we evaluated a particularly challenging scenario involving an 8° camera rotation. While the image stabilization technique successfully aligned images within half the grid pitch period, substantial measurement errors persisted. These results indicate that projective transformation-based image stabilization becomes less effective under large rotations, highlighting the need for further compensation to improve robustness in extreme conditions.

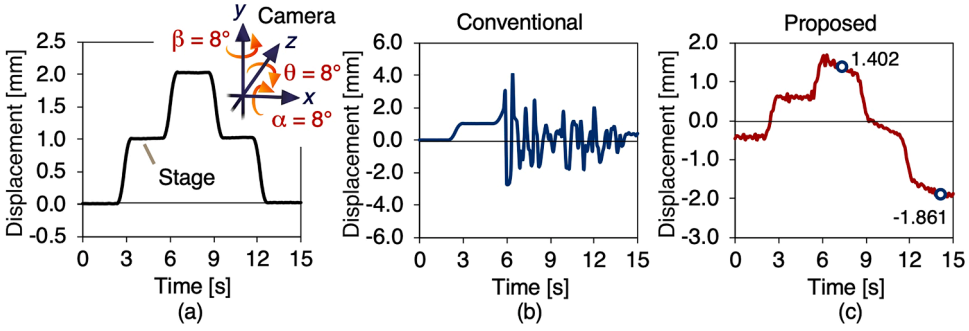

Fig. 15. Experimental results with the camera simultaneous rotated 8 ° for three-axis: (a) actual displacement in *y*-direction when the camera rotation angle is 8 ° around *xyz*-axes, (b) measured displacement by conventional sampling moiré method calculation, and (c) measured displacement by the proposed method with image stabilization.

5. Conclusions

In this study, we proposed a novel approach to efficiently compensate for camera motion, enabling accurate measurement of true structural displacements. Our key contributions are as follows:

(1) We utilize the sampling moiré method, achieving an exceptional accuracy of 1/100 pixel, providing a robust foundation for both motion compensation and displacement measurement.
(2) We developed a two-stage processing framework that effectively eliminates camera-induced motions while preserving actual displacements.
(3) To validate our methodology, we systematically design and conduct experiments that investigate critical parameters for image stabilization, demonstrating its effectiveness through comprehensive comparisons.

The proposed motion compensation method has significant potential for improving infrastructure maintenance efficiency through deployment with various optical devices, including handheld camera, smartphones, and drones. It offers broad applicability for high-precision, low-cost, displacement monitoring with high flexibility.

CRediT authorship contribution statement

Shien Ri: Writing – original draft, Visualization, Validation, Methodology, Investigation, Conceptualization. **Hiroto Oouchi:** Writing – original draft, Software, Data curation. **Jiaxing Ye:** Writing – review & editing, Investigation, Conceptualization. **M.J. Mohammad Fikry:** Writing – review & editing. **Shinji Ogihara:** Writing – review & editing, Supervision.

Declaration of competing interest

The authors declare that they have no known competing financial interests or personal relationships that could have appeared to influence the work reported in this paper.

Acknowledgements

The authors thank Ms. Y. Noguchi for the figure drawing.

Data availability

Data will be made available on request.

References

[1] America's infrastructure Report Card https://infrastructurereportcard.org/(2021).
[2] Japan's Infrastructure Grades 2020 & Introduction of Maintenance Technologies, Japan Society of Civil Engineers (JSCE), https://www.jsce-int.org/node/733.
[3] White paper on land, infrastructure, transport and tourism in Japan, https://www.mlit.go.jp/hakusyo/mlit/r04/hakusho/r05 (2023).
[4] Gindy M, Vaccaro R, Nassif H, Velde J. A state-space approach for deriving bridge displacement from acceleration. Comput Aided Civ Infrastruct Eng 2008;23:281–90.
[5] Masri SF, et al. Experimental study of embedded fiber-optic strain gauges in concrete structures. J Eng Mech 1994;120:1696–717.
[6] Hou X, Yang X, Huang Q. Using inclinometers to measure bridge deflection. J Bridge Eng 2005;10. 564-560.
[7] Psimoulis PA, Stiros SC. Measuring deflections of a short-span railway bridge using a robotic total station. J Bridge Eng 2013;18:182–5.
[8] Chan T, Yu L, Tam H, Ni Y, Liu S, Chung W, Cheng L. Fiber Bragg grating sensors for structural health monitoring of Tsing Ma bridge: background and experimental observation. Eng Struct 2006;28(5):6480659.
[9] Albrecht HE, Borys M, Damaschke N, Tropea C. Laser doppler and phase doppler measurement techniques. Heidelberg: Springer Berlin; 2003.
[10] Rashidi M, et al. A decade of modern bridge monitoring using terrestrial laser scanning: review and future directions. Remote Sens 2020;12:3796.
[11] Shang Y, Yu Q, Yang Z, Xu Z, Zhang X. Displacement and deformation measurement for large structures by camera network. Opt Laser Eng 2014;54:247–54.
[12] Ri S, Wang Q, Tsuda H, Shirasaki H, Kuribayashi K. Displacement measurement of concrete bridges by the sampling Moiré method based on phase analysis of repeated pattern. Strain 2020;56:e12351.
[13] Ri S, Tsuda H, Chang K, Lo F, Lee T. Dynamic deformation measurement by the sampling moiré method from video recording and its application to bridge engineering. Exp Tech 2020;44:313–27.
[14] Ri S, Wang Q, Tsuda H, Shirasaki H, Kuribayashi K. Deflection measurement of bridge using images captured under the bridge by sampling moiré method. Exp Tech 2023;47:1085–95.
[15] Wu H, Zhang X, Gan J, Li H, Ge P. Displacement measurement system for inverters using computer micro-vision. Opt Laser Eng 2016;81:113–8.
[16] Wang Q, Ri S, Xia P, Liu Z. Automatic detection of defect positions including interface dislocations and strain measurement in Ge/Si heterostructure from moiré phase processing of TEM image. Opt Laser Eng 2020;129:106077.
[17] Wang Q, Ri S, Xia P, Ye J, Toyama N. Point defect detection and strain mapping in Si single crystal by two-dimensional multiplication moiré method. Nanoscale 2021;13(40):16900–8.
[18] Wang Q, Ri S, Fikry M, Ogihara S. Multiplication sampling moiré method for full-field deformation measurement of composite materials. Opt Lett 2022;47(1):70–3.
[19] Aguilar A, Davila A, Landgrave J. Displacement measurement with multi-level spiral phase filtering in speckle interferometry. Opt Laser Eng 2014;52:19–26.
[20] Chen R, Zhang C, Shi W, Xie H. 3D sampling moiré measurement for shape and deformation based on the binocular vision. Optics Laser Technoly 2023;167:109666.
[21] Yang Y, et al. Blind identification of full-field vibration modes from video measurements with phase-based video motion magnification. Mech Syst Signal Process 2017;85:567–90.
[22] Luo L, Feng MQ, Wu ZY. Robust vision sensor for multi-point displacement monitoring of bridges in the field. Eng Struct 2018;163:255–66.
[23] Lydon D, et al. Development and field testing of a vision-based displacement system using a low-cost wireless action camera. Mech Syst Signal Process 2019;121:343–58.
[24] Dong CZ, Bas S, Catbas FN. Investigation of vibration serviceability of a footbridge using computer vision-based methods. Eng Struct 2020;224:111224.
[25] Jiang W, Fujigaki M, Uchida Y, Funaki S. Measurement of out-of-plane displacement in time series using laser lines and a camera with a diffraction grating. Opt Laser Eng 2022;151:106891.
[26] Kemao Q. Two-dimensional windowed fourier transform for fringe pattern analysis: principles, applications and implementations. Opt Lasers Eng 2007;45:304–17.
[27] Liu ZW, Huang XF, Xie HM, Lou XH, Du H. The artificial periodic lattice phase analysis method applied to deformation evaluation of TiNi shape memory alloy in micro scale. Meas Sci Technolo 2011;22:125702.
[28] Huang X, Dong H, Liu Z, Zhao Y. Probing micro-newton forces on solid/liquid/GaS interfaces using transmission phase shift. Langmuir 2019;35:5442–7.
[29] Wen H, Dong Ruikun, Dong P. Application of deep learning on structure displacement measurement and accuracy analysis. Opt Laser Eng 2024;178:108218.
[30] Wen H, Dong R, Dong P. Structural displacement measurement using deep optical flow and uncertainty analysis. Opt Laser Eng 2024;181:108364.
[31] Weng Y, Lu Z, Spencer Jr BF. Visual–inertial structural acceleration measurement. Comput Aided Civ Infrastruct Eng 2022;37(9):1146–59.
[32] Yoon H, Shin J, Spencer Jr BF. Structural displacement measurement using an unmanned aerial system. Comput Aided Civ Infrastruct Eng 2018;33:183–92.
[33] Ribeiro D, Santos R, Cabral R, Saramago G, Montenegro P, Carvalho H, Correia J, Calcada R. Non-contact structural displacement measurement using Unmanned Aerial Vehicles and video-based systems. Mech Syst Sig Process 2021;160:107869.
[34] Perry BJ, Guo Y. A portable three-component displacement measurement technique using an unmanned aerial vehicle (UAV) and computer vision: A proof of concept. Measurement 2021;176:109222.
[35] Ri S, Ye J, Toyama N, Ogura N. Drone-based displacement measurement of infrastructures utilizing phase information. Nat Commun 2024;15:395. Article number.
[36] Ye J, Ri S. Phase-based motion analysis for high-precision measurement of bridge deflection using drone imagery. Mech Syst Signal Process 2025;228:112433.
[37] Jana D, Nagarajaiah S. Computer vision-based real-time cable tension estimation in Dubrovnik cable-stayed bridge using moving handheld video camera. Struct Control Health Monit 2021;28(5):e2713.
[38] Lavezzi G, Ciarcia M, Won K, Tazarv M. A DIC-UAV based displacement measurement technique for bridge field testing. Eng Struct 2024;308:117951.
[39] Li M, Liu G, Mao Z, Lei Z, Yang Q. Two-dimensional structural motion estimation via analytical signal enhancement of phase-based video processing. J Sound Vib 2023;553:117630.
[40] Guo L, Guo W, Chen D, Duan B, Shi Z. Structural vibration measurement based on improved phase-based motion magnification and deep learning. Mech Syst Signal Process 2025;224:111945.
[41] Zhang Y, Miyamori Y, Mikami S, Saito T. Vibration-based structural state identification by a 1-dimensional convolutional neural network. Comput Aided Civ Infrastruct Eng 2019;34(9):822–39.
[42] Ri S, Fujigaki M, Morimoto Y. Sampling moiré method for accurate small deformation distribution measurement. Exp Mech 2010;50:501–8.

[43] Ri S, Muramatsu T. Theoretical error analysis of the sampling moiré method and phase compensation methodology for single-shot phase analysis. Appl Opt 2012;51 (16):3214–23.
[44] Wang Q, Ri S. Sampling moiré method for full-field deformation measurement: a brief review. Theor Appl Mech Lett 2022;12:100327.
[45] Ri S, Yoshida T, Tsuda H, Sato E. Optical three-dimensional displacement measurement based on moiré methodology and its application to space structures. Opt Laser Eng 2022;148:106752.